ISSN (Print) 1226-1750
ISSN (Online) 2233-6656
**Journal of Magnetics** 18(2), 95-104 (2013) http://dx.doi.org/10.4283/JMAG.2013.18.2.095

# General Analytical Method for Magnetic Field Analysis of Halbach Magnet Arrays Based on Magnetic Scalar Potential

**Ping Jin[1]*, Yue Yuan[1], Heyun Lin[2], Shuhua Fang[2], and S. L. Ho[3]**

[1]*Department of Energy and Electrical Engineering, Hohai University, Nanjing 210098, P. R. China*
[2]*Servo Control Engineering Center of Education Ministry, Southeast University, Nanjing 210096, China*
[3]*Department of Electrical Engineering, Hong Kong Polytechnic University, Kowloon, Hong Kong*

(Received 7 September 2012, Received in final form 13 May 2013, Accepted 27 May 2013)

**This paper presents a general analytical method for predicting the magnetic fields of different Halbach magnet arrays with or without back iron mounted on slotless permanent magnet (PM) linear machines. By using Fourier decomposition, the magnetization components of four typical Halbach magnet arrays are determined. By applying special synthetic boundary conditions on the PM surfaces, the expressions of their magnetic field distributions are derived based on the magnetic scalar potential (MSP), which are simpler than those based on the magnetic vector potential (MVP). The correctness of the method is validated by finite element analysis. The harmonics of airgap flux density waveforms of these Halbach magnet arrays with or without back iron are also compared and optimized.**

**Keywords :** halbach magnet array, magnetic scalar potential, synthetic boundary condition, harmonic analysis

## 1. Introduction

With the development of modern permanent magnet (PM) machines, linear planar and tubular PM machines with Halbach magnet arrays, which offer high efficiency, high power/force density and excellent servo characteristics, have become increasingly attractive for many applications, such as in manufacturing automation, electrical power generation, transportation, healthcare, and household appliances [1-3].

The design optimization and dynamic modeling of such linear planar and tubular PM machines as shown Fig. 1 rely largely on the accurate prediction of their magnetic field distributions by an appropriate method such as, analytical solution, lumped parameter magnetic circuit (LPMC) method or numerical techniques.

The LPMC method as a conventional approach, which can establish the basic relationships between design parameters and machine performances, is often preferred at the initial design stage [4, 5]. However, the LPMC models of the machines are generally dependent on their geometric parameters and rotor positions, hence the flux leakages of these machines are difficult to estimate accurately.

Numerical techniques, such as the finite-element method (FEM), which can provide accurate field distributions by considering the ferromagnetic materials' saturation and complicated boundary conditions, are widely used in the refinement and optimization stages [6-8]. However, numerical techniques are time-consuming, especially for optimization problems, and they cannot normally provide an insightful relationship between design parameters and machine performances.

Analytical solutions derived from the Maxwell equations and simplified boundary conditions, which are more accurate than LPMC method and more insightful than numerical techniques, are accordingly researched and used widely [9-24]. Boules [9, 10] presents an analytical model of a multi-pole PM motor in the two-dimensional (2D) Cartesian coordinate system using an equivalent magnet pole-arc based on the magnetic scalar potential (MSP). Zhu and Howe [11, 12] propose an improved analytical technique for the calculation of the open-circuit air gap field distribution in the 2D polar coordinate system for both internal and external rotor topologies based on the MSP. Amara and Barakat [13] develop a general 2D analytical model to obtain the exact analytical solution of the magnetic field distributions inside the slots as well as in the airgap and the PM regions of slotted tubular and linear


*Corresponding author: Tel: +86-158-05158665
Fax: +86-025-83791696, e-mail: seueelab_jp@163.com

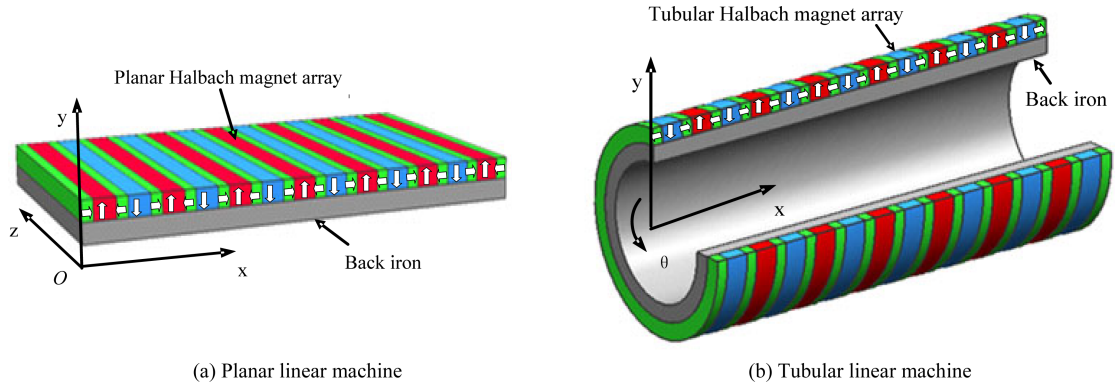


**Fig. 1.** (Color online) Linear machines with Halbach magnetized arrays.

PM machines. Trumper *et al.* [14] provide an analytical method using an equivalent triangular winding for predicting the 2D flux distributions of linear and planar Halbach PM machines based on magnetic vector potential (MVP). Lee *et al.* [15] analyze the magnetic field distribution on the surface of slotless Halbach linear machines without back iron using image method and superposition principle. Wang and Howe [16, 17] present analytical expressions of magnetic field distributions with a quasi-Halbach magnetized armature for both non-ferromagnetic and ferromagnetic supporting tubes based on the MVP. Starting with Maxwell's equations, Pfister and Perriard [18] develop the analytical expression of the vector potential and the magnetic field at any point of a layer cylindrical system. [19-24] are also examples which calculate magnetic flux using MSP. However, all of the analytical analyses based on the MSP are only focusing on the parallel or radial magnetization topologies of the PM arrays in the low permeability regions, as expressions of analytical analyses of Halbach magnetization topologies based on MVP are very complicated.

The purpose of this paper is to present a general analytical method for the analysis of magnetic fields of Halbach PM arrays with or without back iron based on MSP in the 2D Cartesian coordinate system. Some analytical expressions for establishing an accurate relationship of the magnetic field distributions of four typical Halbach magnet arrays with their geometry parameters, which are verified using FEM, are reported in this paper. Comparisons on the harmonics and optimized waveforms of the air gap flux density of these Halbach magnet arrays are also presented.

## 2. Magnetization of Halbach Magnet Arrays

While the slotted stator model has been established as an extension of the slotless stator model by considering the relative permeance or slot correction factor in many studies [25, 26], the focus of this paper is restricted to the analysis of slotless stator by assuming a smooth stator surface based on the following assumptions:

1) The magnetic field distributions is determined from the product of the magnetic field intensity produced by the magnets and relative permeance at any position;

2) The lengths of cyclical Halbach magnet arrays and the cores of the machines in the z direction are assumed to be infinite;

3) The boundary condition on the surface where $y = y_s$ ($y_s$ is the inner surface of the stator iron) as shown in Fig. 2 is the Neumann boundary conditions by assuming the permeability of iron is far larger than that of air. By neglecting flux leakage in the back air region, the boundary condition where $y = y_r$ ($y_r$ is the outer surface of the back iron region) as shown in Fig. 2 is therefore the Dirichlet boundary conditions;

4) The back iron is unsaturated and eddy current and hysteresis loss in it are all neglected;

5) All magnets operate on a linear demagnetization curve.

Fig. 2 shows four typical topologies of Halbach magnet arrays with back iron in linear PM machines, which are discrete in Fig. 2(a), (b) and (c), and ideal in Fig. 2(d). Each of these topologies include five regions which are, namely, the air-gap region I, PM region II, back iron region III, back air region IV, and stator iron region V. The boundary conditions where $y = y_s$ and $y = y_o$ ($y_o$ is the inner surface of the back iron), are, respectively, corresponding to the Neumann and the Dirichlet boundary conditions.

For linear PM machines, the flux density vector $\vec{B}$ and magnet field intensity vector $\vec{H}$ in regions I, II and III, are respectively coupled by

$$\vec{B}_{\mathrm{I}} = \mu_0 \vec{H}_{\mathrm{I}} \tag{1a}$$

$$\vec{B}_{\mathrm{II}} = \mu_0 \mu_r \vec{H}_{\mathrm{II}} + \mu_0 \vec{M} \tag{1b}$$

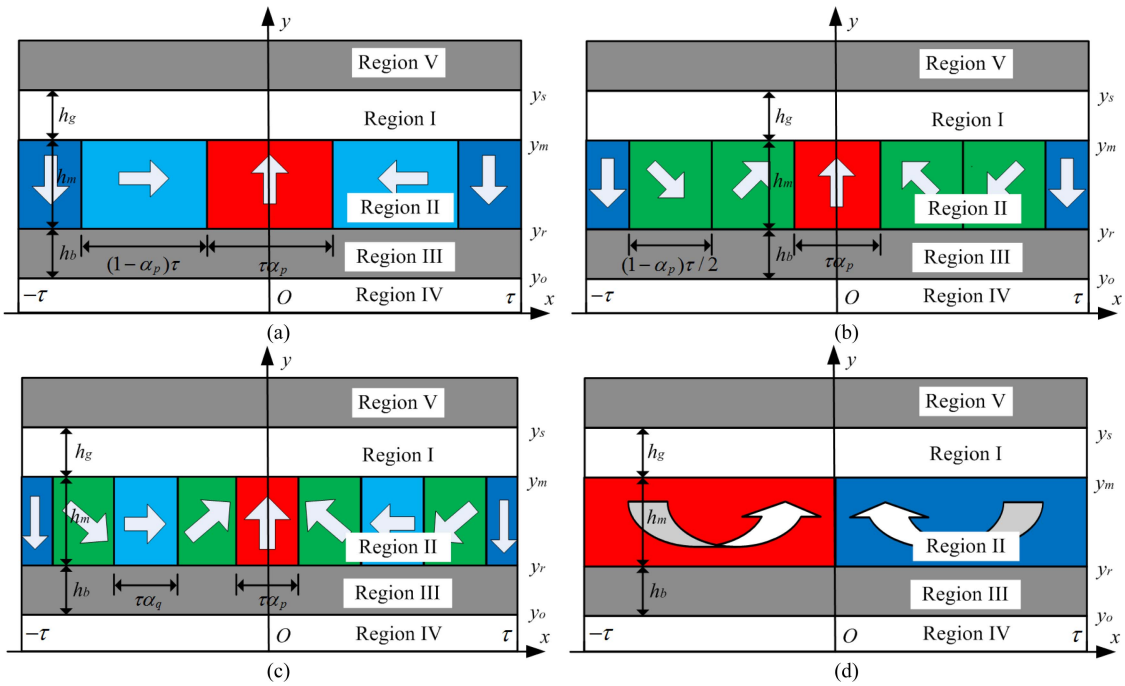


**Fig. 2.** (Color online) Halbach magnet arrays: (a) Two segments, (b) Three segments, (c) Four segments, and (d) Ideal.

$$\vec{B}_{\mathrm{III}} = \mu_0 \mu_{iron} \vec{H}_{\mathrm{III}} \tag{1c}$$

where $\mu_0$ is the permeability of air; $\mu_r$ is the relative permeability of PM; $\mu_{iron}$ is the relative permeability of iron; $\vec{M}$ is the residual magnetization vector of PM.

The amplitude of the residual magnetization vector $\vec{M}$ is given by

$$M = B_r / \mu_0 \tag{2}$$

where $B_r$ is the remanence of permanent magnet.

As the magnetization of PM is uniform, the vector expressions (1) can be replaced by the scalar expressions as

$$B_{\mathrm{I}} = \mu_0 H_{\mathrm{I}} \tag{3a}$$

$$B_{\mathrm{II}} = \mu_0 \mu_r H_{\mathrm{II}} + \mu_0 M \tag{3b}$$

$$B_{\mathrm{III}} = \mu_0 \mu_{iron} H_{\mathrm{III}} \tag{3c}$$

In the 2D Cartesian coordinate system, the residual magnetization vector can be decomposed as

$$\vec{M} = M_x \vec{x} + M_y \vec{y} \tag{4}$$

where $M_x = M \cos\theta$ and $M_y = M \sin\theta$. $M_x$ and $M_y$ are respectively the x and y direction component of $\vec{M}$.

### 2.1. Two-segment Halbach magnet array

The magnetization components of the PMs in Fig. 2(a) are given in Table 1, where $\alpha_p$ is the ratio of the x-direction length of the y-direction magnetized PM to a pole length $\tau$. Using the Fourier series method, the distributions of magnetization components $M_x$ and $M_y$ in (4) can be expressed by

$$M_x = \sum_{k=1,3,5\ldots}^{\infty} M_{xk} \sin\left(\frac{k\pi}{\tau}x\right) \tag{5a}$$

$$M_y = \sum_{k=1,3,5\ldots}^{\infty} M_{yk} \cos\left(\frac{k\pi}{\tau}x\right) \tag{5b}$$

where

**Table 1.** The Magnetization Components of the PMs in Fig. 2(a)

| Boundary | $M_x$ | $M_y$ |
|---|---|---|
| $-\tau < x < -\frac{\tau(2-\alpha_p)}{2}$ | 0 | $-\frac{B_r}{\mu_0}$ |
| $-\frac{\tau(2-\alpha_p)}{2} < x < -\frac{\tau\alpha_p}{2}$ | $\frac{B_r}{\mu_0}$ | 0 |
| $-\frac{\tau\alpha_p}{2} < x < -\frac{\tau\alpha_p}{2}$ | 0 | $\frac{B_r}{\mu_0}$ |
| $\frac{\tau\alpha_p}{2} < x < \frac{\tau(2-\alpha_p)}{2}$ | $-\frac{B_r}{\mu_0}$ | 0 |
| $\frac{\tau(2-\alpha_p)}{2} < x < \tau$ | 0 | $-\frac{B_r}{\mu_0}$ |

**Table 2.** The Magnetization Components of the PMs In Fig. 2(b)

| Boundary | | |
|---|---|---|
| $-\tau < x < -\frac{\tau(2-\alpha_p)}{2}$ | 0 | $-\frac{B_r}{\mu_0}$ |
| $-\frac{\tau(2-\alpha_p)}{2} < x < -\frac{\tau}{2}$ | $\delta_x\frac{B_r}{\mu_0}$ | $-\delta_y\frac{B_r}{\mu_0}$ |
| $-\frac{\tau}{2} < x < -\frac{\tau\alpha_p}{2}$ | $\delta_x\frac{B_r}{\mu_0}$ | $\delta_y\frac{B_r}{\mu_0}$ |
| $-\frac{\tau\alpha_p}{2} < x < -\frac{\tau\alpha_p}{2}$ | 0 | $\frac{B_r}{\mu_0}$ |
| $\frac{\tau\alpha_p}{2} < x < -\frac{\tau}{2}$ | $-\delta_x\frac{B_r}{\mu_0}$ | $\delta_y\frac{B_r}{\mu_0}$ |
| $\frac{\tau}{2} < x < \frac{\tau(2-\alpha_p)}{2}$ | $-\delta_x\frac{B_r}{\mu_0}$ | $-\delta_y\frac{B_r}{\mu_0}$ |
| $\frac{\tau(2-\alpha_p)}{2} < x < \tau$ | 0 | $-\frac{B_r}{\mu_0}$ |

$$M_{xk} = \frac{4B_r}{\mu_0 k\pi}A_{xk} \quad M_{yk} = \frac{4B_r}{\mu_0 k\pi}A_{yk} \tag{6}$$

and

$$A_{xk} = \sin\frac{k\pi}{2}\sin\frac{k\pi(1-\alpha_p)}{2} \qquad A_{yk} = \sin\frac{\pi k\alpha_p}{2} \tag{7}$$

where $A_{xk}$ and $A_{yk}$ are defined as the magnetization distribution factors of the Halbach magnet arrays in the $x$ and $y$ directions, respectively.

### 2.2. Three-segment Halbach magnet array

The magnetization components of the PMs in Fig. 2(b) are shown in Table 2, where $\delta_x = |\sin\theta|$, $\delta_y = |\cos\theta|$ and $\theta$ is the angle of the angular magnetic PM. Using the Fourier series method, the distributions of magnetization components $M_x$ and $M_y$ can also be expressed by (5). However their magnetization distribution factors are changed to

$$A_{xk} = \delta_x \sin\frac{k\pi}{2}\sin\frac{k\pi(2-\alpha_p)}{2} \tag{8a}$$

$$A_{yk} = \sin\frac{\pi k\alpha_p}{2} - \delta_y \sin\frac{k\pi(1-\alpha_p)}{2} \tag{8b}$$

### 2.3. Four-segment Halbach magnet array

The magnetization components of the PMs in Fig. 2(c) are given in Table 3, where $\delta_x = |\sin\theta|$, $\delta_y = |\cos\theta|$ and $\alpha_q$ is the ratio of the x-direction length of the x-direction magnetized PM to a pole length $\tau$. Using the Fourier series method, the distributions of magnetization components $M_x$ and $M_y$ can also be expressed by (5), but their distribution factors are changed to

**Table 3.** The Magnetization Components of the PMs in Fig. 2(c)

| Boundary | $M_x$ | $M_y$ |
|---|---|---|
| $-\tau < x < -\frac{\tau(2-\alpha_p)}{2}$ | 0 | $-\frac{B_r}{\mu_0}$ |
| $-\frac{\tau(2-\alpha_p)}{2} < x < -\frac{\tau(1+\alpha_q)}{2}$ | $\delta_x\frac{B_r}{\mu_0}$ | $-\delta_y\frac{B_r}{\mu_0}$ |
| $-\frac{\tau(1+\alpha_q)}{2} < x < -\frac{\tau(1-\alpha_q)}{2}$ | $\frac{B_r}{\mu_0}$ | 0 |
| $-\frac{\tau(1-\alpha_q)}{2} < x < -\frac{\tau\alpha_p}{2}$ | $\delta_x\frac{B_r}{\mu_0}$ | $\delta_y\frac{B_r}{\mu_0}$ |
| $-\frac{\tau\alpha_p}{2} < x < -\frac{\tau\alpha_p}{2}$ | 0 | $\frac{B_r}{\mu_0}$ |
| $\frac{\tau\alpha_p}{2} < x < \frac{\tau(1-\alpha_q)}{2}$ | $-\delta_x\frac{B_r}{\mu_0}$ | $\delta_y\frac{B_r}{\mu_0}$ |
| $\frac{\tau(1-\alpha_q)}{2} < x < \frac{\tau(1+\alpha_q)}{2}$ | $-\frac{B_r}{\mu_0}$ | 0 |
| $\frac{\tau(1+\alpha_q)}{2} < x < \frac{\tau(2-\alpha_p)}{2}$ | $-\delta_x\frac{B_r}{\mu_0}$ | $-\delta_y\frac{B_r}{\mu_0}$ |
| $\frac{\tau(2-\alpha_p)}{2} < x < \tau$ | 0 | $-\frac{B_r}{\mu_0}$ |

$$A_{xk} = -\sin\frac{k\pi}{2}\sin\frac{k\pi\alpha_q}{2} + \delta_x \sin\frac{k\pi(1+\alpha_p-\alpha_q)}{4}\sin\frac{k\pi(1+\alpha_q-\alpha_p)}{4} \tag{9a}$$

$$A_{yk} = \sin\frac{\pi k\alpha_q}{2} + \delta_y \cos\frac{k\pi(1+\alpha_p-\alpha_q)}{4}\sin\frac{k\pi(1-\alpha_q-\alpha_p)}{4} \tag{9b}$$

### 2.4. Ideal Halbach magnet array

The magnetization components of the PMs in Fig. 2(d) are shown in Table 4. Using the Fourier series method, the distributions of magnetization components $M_x$ and $M_y$ can still be expressed by (5), and their distribution factors are given by

$$A_{xk} = A_{yk} = \frac{\pi}{4} \tag{10}$$

For all Halbach magnet arrays, $M_x$ is a homogeneous harmonic odd function and $M_y$ is a homogeneous harmonic

**Table 4.** The Magnetization Components of the PMs in Fig. 2(d)

| $M_x$ | $M_y$ |
|---|---|
| $-\frac{B_r}{\mu_0}\sin\frac{\pi x}{\tau}$ | $\frac{B_r}{\mu_0}\cos\frac{\pi x}{\tau}$ |

even function. Using the Fourier series method, the distributions of magnetization components $M_x$ and $M_y$ can be expressed by (5) together with different distribution factors.

## 3. Magnetic Field Distribution

In terms of the MSP function $\varphi$

$$H_x = -\frac{\partial \varphi}{\partial x} \text{ and } H_y = -\frac{\partial \varphi}{\partial x} \tag{11}$$

where $H_x$ and $H_y$ are respectively the x and y direction component of $\vec{H}$.

The MSP distributions in regions I, II and III are all governed by the Laplace equation, i.e.,

$$\frac{\partial^2 \varphi}{\partial x^2} + \frac{\partial^2 \varphi}{\partial y^2} = 0 \tag{12}$$

The general solution for the MSP in these regions has the form

$$\varphi_n(x,y) = \sum_{k=1}^{\infty} (A_{nk}e^{\omega y} + B_{nk}e^{-\omega y})(C_{nk}\sin\omega x + D_{nk}\cos\omega x) + A_{n0}xy + B_{n0}x + C_{n0}y + D_{n0} \tag{13}$$

where $A_{nk}$, $B_{nk}$, $C_{nk}$, $D_{nk}$, $A_{n0}$, $B_{n0}$, $C_{n0}$, $D_{n0}$ are the constant in the different region ($n$ is I, II or III). Due to the homogeneous harmonic characters of the distributions of magnetization components $M_x$ and $M_y$, can be reduced as

$$\varphi_n(r,z) = \sum_{k=1,3,5}^{\infty} \left(A_{nk}e^{k\frac{\pi}{\tau}y} + B_{nk}e^{-k\frac{\pi}{\tau}y}\right)\cos\left(k\frac{\pi}{\tau}x\right) \tag{14}$$

For the PM linear machine with back air region IV, the boundary conditions for $y = y_s$ and $y = y_0$ are, respectively, the Neumann and the Dirichlet boundary conditions. For the tubular PM linear machine without region IV, Fig. 2(b) is changed to Fig. 3 as an example, and the boundary condition for $y = 0$ is the Dirichlet boundary condition. For the planar or tubular PM linear machines without back iron, the relative permeability $\mu_{rion}$ of region III in Fig. 3

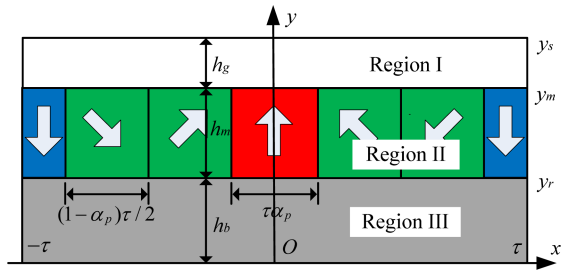


**Fig. 3.** (Color online) Three segments Halbach magnet array with one back region.

is replaced by $\mu_0$ and the boundary condition for $y = 0$ is also the Dirichlet boundary condition. Thus, the boundary conditions for $y = y_s$ and $y = y_0$ of Fig. 2 are given by

$$B_{x1}(x,y)|_{y=y_s} = 0 \tag{15a}$$

$$B_{y\text{III}}(x,y)|_{y=y_0} = 0 \tag{15b}$$

where $B_x$ and $B_y$ are respectively the x and y direction component of $\vec{B}$.

If both $B_{x\text{II}}(x, y)$ and $B_{y\text{II}}(x, y)$ are governed by (3b), the boundary conditions between $y_r$ and $y_m$ will be very complex and hence the expressions of the magnetic field distributions will be difficult solved. In this paper, the synthetic boundary conditions as shown in Fig. 4(a) are presented. For $y = y_r$ and $y = y_m$, $M_y$ is governed by (3b), whereas $M_x$ is replaced by a virtual equivalent surface current $J_s$, which is given by

$$J_s = M_x/\mu_r \tag{16}$$

thus, Fig. 2(b) is equivalent to Fig. 4(b) as an illustrating example.

The synthetic boundary conditions for $y = y_r$ and $y = y_m$ in Fig. 2 are defined by

$$H_{x1}(x,y)|_{y=y_m} = H_{x\text{II}}(x,y)|_{y=y_m} + M_x/\mu_r \tag{17c}$$

$$B_{y1}(x,y)|_{y=y_m} = B_{y\text{II}}(x,y)|_{y=y_m} \tag{17d}$$

$$H_{x\text{III}}(x,y)|_{y=y_r} = H_{x\text{II}}(x,y)|_{y=y_r} + M_x/\mu_r \tag{17e}$$

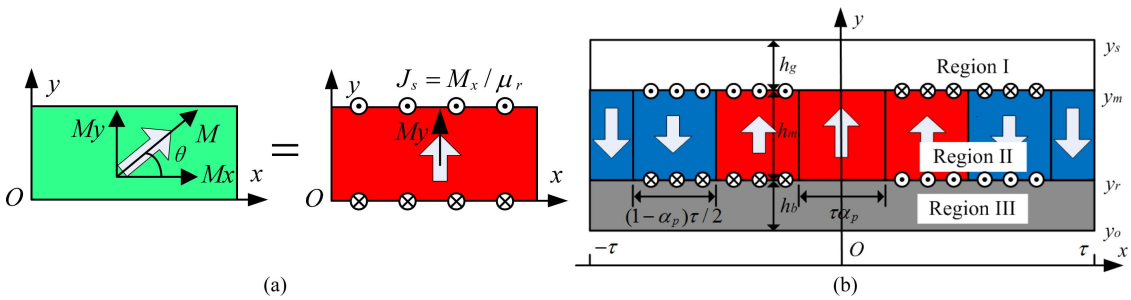


**Fig. 4.** (Color online) Synthetic boundary conditions.

$$B_{y\mathrm{III}}(x,y)\big|_{y=y_r} = B_{y\mathrm{II}}(x,y)\big|_{y=y_r} \tag{17f}$$

By solving (14), subject to the distributions of magnetization components (5) and the boundary conditions of (15) and (17), the general solutions in the three regions and on the surface of the stator core are expressed as follows:

In air-gap region I

$$B_{x\mathrm{I}}(x,y) = \sum_{k=1,3,5}^{\infty} \frac{4B_r}{\pi k}\left(A_{yk} - \frac{E_bE_d - e^{-k\frac{\pi}{\tau}h_m}E_eE_a + e^{-k\frac{\pi}{\tau}h_m}E_eE_c - e^{-2k\frac{\pi}{\tau}h_m}E_bE_f}{E_cE_d - e^{-2k\frac{\pi}{\tau}h_m}E_fE_a}\right)e^{-k\frac{\pi}{\tau}(y_m-y)}$$

$$\frac{\left(e^{2k\frac{\pi}{\tau}(y-y_s)}-1\right)}{\left(e^{-2k\frac{\pi}{\tau}h_g}+1\right)}\sin\frac{k\pi}{\tau}x \tag{18a}$$

$$B_{y\mathrm{I}}(x,y) = \sum_{k=1,3,5}^{\infty} \frac{4B_r}{\pi k}\left(A_{yk} - \frac{E_bE_d - e^{-k\frac{\pi}{\tau}h_m}E_eE_a + e^{-k\frac{\pi}{\tau}h_m}E_eE_c - e^{-2k\frac{\pi}{\tau}h_m}E_bE_f}{E_cE_d - e^{-2k\frac{\pi}{\tau}h_m}E_fE_a}\right)e^{-k\frac{\pi}{\tau}(y_m-y)}$$

$$\frac{\left(e^{2k\frac{\pi}{\tau}(y-y_s)}+1\right)}{\left(e^{-2k\frac{\pi}{\tau}h_g}+1\right)}\cos\frac{k\pi}{\tau}x \tag{18b}$$

In PM region II

$$B_{x\mathrm{II}}(x,y) = -\sum_{k=1,3,5}^{\infty} \frac{4B_r}{\pi k}$$

$$\frac{e^{k\frac{\pi}{\tau}(y-y_m)}E_bE_a - e^{k\frac{\pi}{\tau}(y-y_m-h_m)}E_eE_a - e^{k\frac{\pi}{\tau}(y_r-y)}E_eE_c + e^{k\frac{\pi}{\tau}(y_r-y-h_m)}E_bE_f}{E_cE_d - e^{-2k\frac{\pi}{\tau}h_m}E_fE_d}\sin\frac{k\pi}{\tau}x \tag{18c}$$

$$B_{y\mathrm{II}}(x,y) = \sum_{k=1,3,5}^{\infty} \frac{4B_r}{\pi k}$$

$$\left[A_{yk} - \frac{e^{k\frac{\pi}{\tau}(y-y_m)}E_bE_d - e^{k\frac{\pi}{\tau}(y-y_m-h_m)}E_eE_a + e^{k\frac{\pi}{\tau}(y_r-y)}E_eE_c - e^{k\frac{\pi}{\tau}(y_r-y-h_m)}E_bE_f}{E_cE_d - e^{-2k\frac{\pi}{\tau}h_m}E_fE_d}\right]\cos\left(\frac{k\pi}{\tau}x\right) \tag{18d}$$

In back iron region III

$$B_{x\mathrm{III}}(r,z) = \sum_{k=1,3,5\ldots}^{\infty} \frac{4B_r}{\pi k}\left(M_1 - \frac{e^{-2k\frac{\pi}{\tau}h_m}E_aE_e - e^{-k\frac{\pi}{\tau}h_m}E_bE_d - E_eE_c + e^{-k\frac{\pi}{\tau}h_m}E_bE_f}{e^{-2k\frac{\pi}{\tau}h_m}E_aE_f - E_cE_d}\right)$$

$$\frac{e^{k\frac{\pi}{\tau}(y-y_r)}\left(1+e^{2k\frac{\pi}{\tau}(y_0-y)}\right)}{\left(e^{-2k\frac{\pi}{\tau}h_g}-1\right)}\sin\left(\frac{k\pi}{\tau}x\right) \tag{18e}$$

$$B_{y\mathrm{III}}(r,z) = \sum_{k=1,3,5\ldots}^{\infty} \frac{4B_r}{\pi k}\left(M_1 - \frac{e^{-2k\frac{\pi}{\tau}h_m}E_aE_e - e^{-k\frac{\pi}{\tau}h_m}E_bE_d - E_eE_c + e^{-k\frac{\pi}{\tau}h_m}E_bE_f}{e^{-2k\frac{\pi}{\tau}h_m}E_aE_f - E_cE_d}\right)$$

$$\frac{e^{k\frac{\pi}{\tau}(y-y_r)}\left(e^{2k\frac{\pi}{\tau}(y_0-y)}-1\right)}{\left(e^{-2k\frac{\pi}{\tau}h_g}-1\right)}\cos\left(\frac{k\pi}{\tau}x\right) \tag{18f}$$

On the surface of the stator, i.e., $y = y_s$

$$B_y(x) = \sum_{k=1,3,5\ldots}^{\infty} \frac{4B_r}{\pi k}\left(A_{yk} - \frac{E_bE_d - e^{-k\frac{\pi}{\tau}h_m}E_eE_a + e^{-k\frac{\pi}{\tau}h_m}E_eE_c - e^{-2k\frac{\pi}{\tau}h_m}E_bE_f}{E_cE_d - e^{-2k\frac{\pi}{\tau}h_m}E_fE_a}\right)$$

$$\frac{2e^{2k\frac{\pi}{\tau}h_g}}{\left(e^{-2k\frac{\pi}{\tau}h_g}+1\right)}\cos\frac{k\pi}{\tau}x \tag{19}$$

where,

$$E_a = \left(e^{-2k\frac{\pi}{\tau}h_g}-1\right) + \frac{1}{\mu_r}\left(e^{-2k\frac{\pi}{\tau}h_g}+1\right)$$

$$E_b = A_{xk}\frac{1}{\mu_r}\left(e^{-2k\frac{\pi}{\tau}h_g}+1\right) + A_{yk}\left(e^{-2k\frac{\pi}{\tau}h_g}-1\right)$$

$$E_c = \left(e^{-2k\frac{\pi}{\tau}h_g}-1\right) - \frac{1}{\mu_r}\left(e^{-2k\frac{\pi}{\tau}h_g}+1\right)$$

$$E_d = \left(1+e^{-2k\frac{\pi}{\tau}h_b}\right) + \frac{\mu_{iron}}{\mu_r}\left(1-e^{-2k\frac{\pi}{\tau}h_b}\right)$$

$$E_e = A_{xk}\frac{\mu_{iron}}{\mu_r}\left(1+e^{-2k\frac{\pi}{\tau}h_b}\right) + A_{yk}\left(1+e^{-2k\frac{\pi}{\tau}h_b}\right)$$

$$E_f = \left(1+e^{-2k\frac{\pi}{\tau}h_b}\right) - \frac{\mu_{iron}}{\mu_r}\left(1-e^{-2k\frac{\pi}{\tau}h_b}\right)$$

where the thickness of the air gap $h_g = y_s - y_m$, the thickness of the Halbach magnet array $h_m = y_m - y_r$, the thickness of the back iron $h_b = y_r - y_o$. When region III is the back air region, $\mu_{iron} = \mu_0$ in (18) and (19).

## 4. Comparison with the Finite Element Analysis

The initial main design parameters of the proposed

**Table 5.** Basic Parameters of Halbach Magnet Arrays

| Parameters | Values |
|---|---|
| $h_g$ | 1 mm |
| $h_m$ | 4 mm |
| $h_b$ | 10 mm |
| $\tau$ | 20 mm |
| $\alpha_p$ | 1/p* |
| $\alpha_q$ | 1/q** |

*$p$ = 2, 3, 4 for the 2, 3, 4 segments Halbach magnet array; **$q$ = 4 for the 4 segments Halbach magnet array.

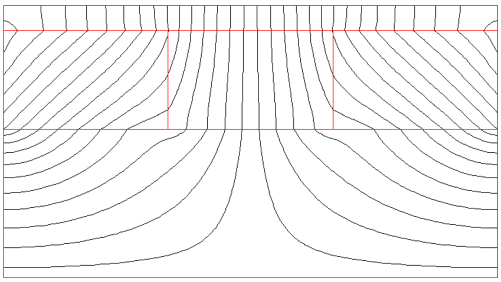

**Fig. 5.** (Color online) Fluxes of the three segments Halbach magnet array with back iron in a half cycle.

Halbach magnet arrays are given in Table 5.

The analytical predictions have been validated by finite element analysis based on MVP by applying the periodic boundary conditions where x = ± $\tau/2$ together with the corresponding boundary conditions where $y = y_s$ and $y = y_o$ or $y = 0$, as shown in Fig. 5. Fig. 6 compares the distributions of the three segments of the Halbach magnet array with back iron in a half cycle, where $y$ is equal to 20.5 mm in air-gap region I, 18 mm in PM region II and 15 mm in back iron region III. It can be seen that the magnetic flux density is essentially zero in the x direction in air-gap region I, and obviously stepped in the y direction in PM region II. All the predicted analytical results are in good agreement with the finite element results.

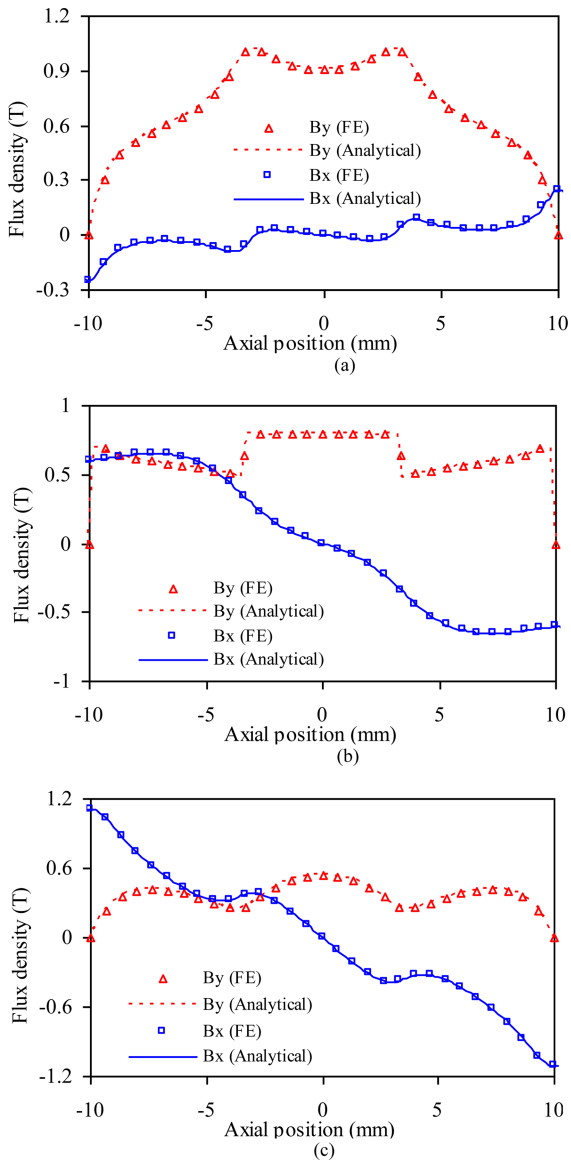


**Fig. 6.** (Color online) Flux densities (a) region I, (b) region II, and (c) region III.

## 5. Harmonics and Magnetic Field Optimization

The analytical predictions can be applied to calculate the harmonics readily by setting $k$ to assume an odd integer number, because there are no even harmonics in the flux density distributions, both in the x and y directions of the Halbach magnetized arrays. The $k$-th component amplitude of the air gap flux density can be calculated by (20), which is obtained from (19) by setting $x = 0$. Fig. 7 shows the flux density distributions in a half cycle where $y = y_s$ together with the harmonic analysis of the four typical Halbach magnet arrays with or without back iron. All values used to compute the magnetic field are the same as those given in Table 5. All the predicted results of the flux densities using the proposed analytical method agree well with the finite element ones. The fundamental amplitudes of the Halbach magnet arrays with back iron are larger than those of the arrays with back air. It can be seen that the harmonics are reduce as the segments number increases.

$$F_k = abs\left\{\frac{4B_r}{\pi k}\left[A_{yk} - \frac{E_bE_d - e^{-k\frac{\pi}{\tau}h_m}E_eE_a + e^{-k\frac{\pi}{\tau}h_m}E_eE_c + e^{-2k\frac{\pi}{\tau}h_m}E_bE_f}{E_cE_d - e^{-2k\frac{\pi}{\tau}h_m}E_fE_a}\right]\frac{2e^{-k\frac{\pi}{\tau}h_g}}{\left(e^{-2k\frac{\pi}{\tau}h_m}+1\right)}\right\}_{k=1,3,5,\ldots} \quad (20)$$

The air-gap field distribution in linear PM machines is required to be sinusoidal in order to produce low cogging torque with minimize speed ripple in order to realise high positional accuracy. The total harmonic distortion (THD) of the magnetic field distributions on the surface of the stator is defined as

$$THD = \frac{\sqrt{\sum_{n=2}^{\infty} F_k}}{F_1} \quad (21)$$

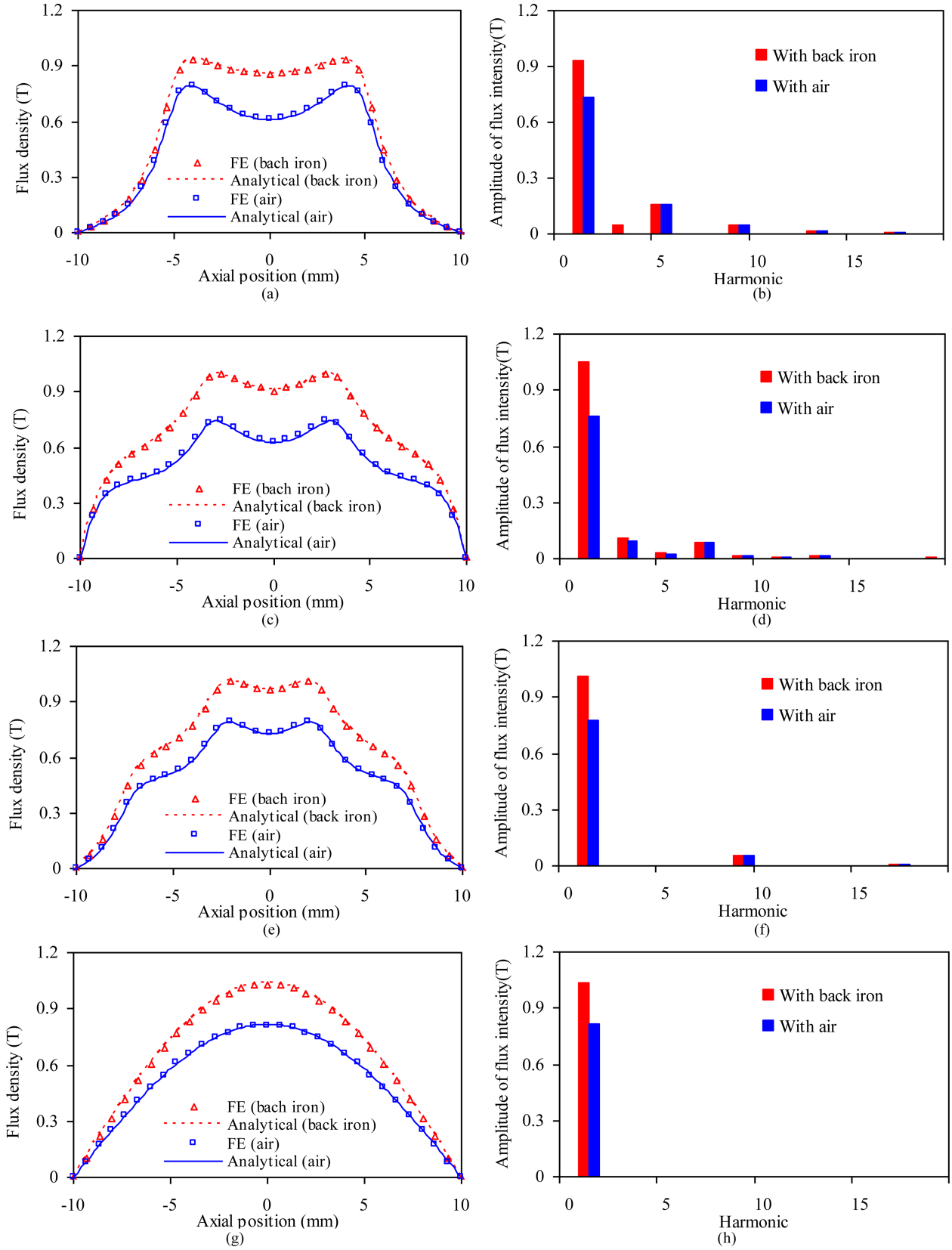


**Fig. 7.** (Color online) Comparison of flux densities and analysis of the harmonics: (a) Two-segment Halbach magnet array, (b) Three-segment Halbach magnet array, (c) Four-segment Halbach magnet array, and (d) Ideal Halbach magnet array.

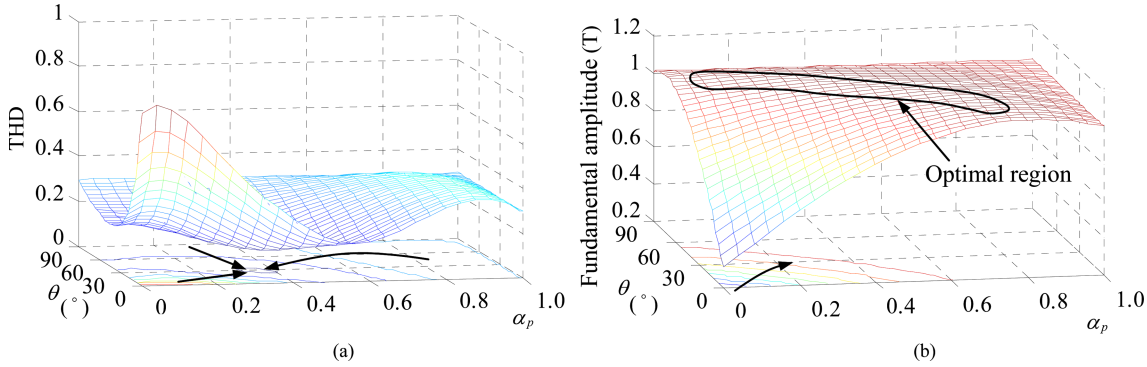


**Fig. 8.** (Color online) Predicted variation of THD and fundamental amplitude of air gap flux density as functions $\alpha_p$ and $\theta$ when the back iron is present.

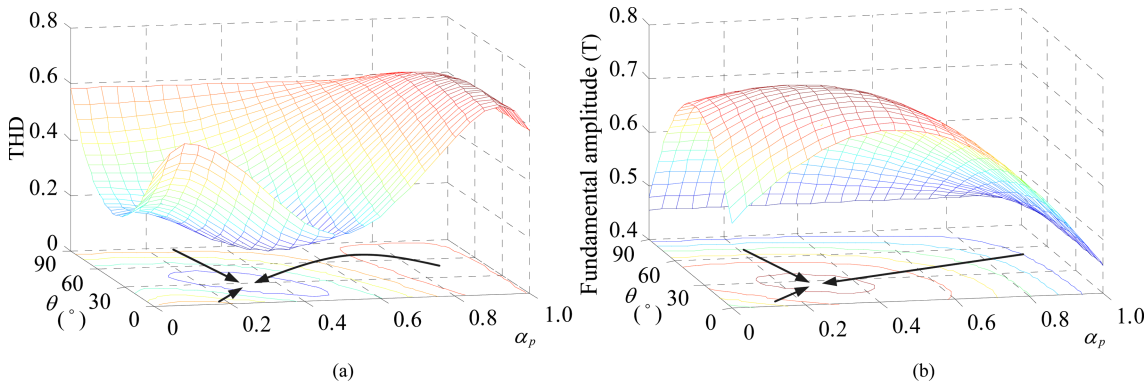


**Fig. 9.** (Color online) Predicted variation of THD and fundamental amplitude of air gap flux density as functions of $\alpha_p$ and $\theta$ when there is no back iron.

**Table 6.** Preferred Results of the Three-Segment Halbach Magnet Array

| Item | THD | FCA(T) | Position |
|---|---|---|---|
| Halbach magnet array with back iron | | | |
| Non-Halbach | 0.2971 | 1.0096 | $\alpha_p = 1$ or $\theta = 90^o$ |
| Initial design | 0.1394 | 1.0492 | $\alpha_p = 0.33$, $\theta = 45^o$ |
| Preferred THD | 0.0932 | 0.9904 | $\alpha_p = 0.35$, $\theta = 29^o$ |
| Preferred FCA | – | 1.0813 | Preferred Region |
| Worst THD | 0.8003 | 0.3701 | $\alpha_p = 0.04$, $\theta = 0^o$ |
| Worst FCA | 0.7650 | 0.3071 | $\alpha_p = 0$, $\theta = 0$ |
| Halbach magnet array without back iron | | | |
| Non-Halbach | 0.5832 | 0.4523 | $\alpha_p = 1$ or $\theta = 90^o$ |
| Initial design | 0.1819 | 0.7367 | $\alpha_p = 0.33$, $\theta = 45^o$ |
| Preferred THD | 0.1218 | 0.7589 | $\alpha_p = 0.33$, $\theta = 30^o$ |
| Preferred FCA | 0.1451 | 0.7615 | $\alpha_p = 0.29$, $\theta = 27^o$ |
| Worst THD | 0.6915 | 0.5307 | $\alpha_p = 0.89$, $\theta = 32^o$ |
| Worst FCA | 0.5832 | 0.4523 | $\alpha_p = 1$, $\theta = 90^o$ |

For the three-segment Halbach magnet array with back iron shown in Fig. 2(b), its analytical predicted variation of THD and fundamental component amplitude of its air gap flux density as functions of $\alpha_p$ and $\theta$, when the thickness and the pole pitch of the Halbach magnet array are fixed, are given in Fig. 8. When $\alpha_p = 0.35$ and $\theta = 29^o$ in (4), the preferred THD is 0.0932 and the preferred fundamental component amplitude ($F_1$) is about 1.096T. When $\alpha_p$ and $\theta$ are changed to zero, the fundamental component amplitude decreases rapidly.

For the three-segment Halbach magnet array without back iron shown in Fig. 3, its analytical predicted variation of THD and fundamental component amplitude of the air gap flux density are given in Fig. 9. It can be seen that both of them have similar preferred points. The preferred THD and fundamental component amplitude is 0.1218 and 0.7615, respectively. When $\alpha_p = 0.89$ and $\theta = 32^o$, the biggest THD is 0.6915. Table 6 gives the preferred results of the three-segment Halbach magnet array with and without back iron.

## 6. Conclusions

A general method for the magnetic field analysis of different Halbach magnet arrays with or without back iron

based on MSP has been established in the 2-D Cartesian coordinate system. It has been reported that the magnetization components of the four typical topologies i.e., two-segment-, three-segment-, four-segment- and ideal Halbach magnet arrays, can be described using the same expressions with different distribution factors. The synthetic boundary conditions on the surface of the Halbach magnet arrays have been presented, based on which the magnetic field expressions of all regions with or without back iron are derived. The predicted magnetic field distributions of the different Halbach topologies are in good agreement with the finite element analysis calculations based on MVP. The harmonic analysis of the flux density waveforms of the four typical Halbach magnet arrays is based on the magnetic field expressions which are obtained using the proposed general method. The THD and fundamental component amplitude of the air gap flux density waveforms are also optimized. The general method as reported in this paper can be used for analyzing magnetic field distributions of any Halbach magnet arrays with or without back iron.

## Acknowledgment

Project supported by National Natural Science Foundation of China (50907007); Specialized Research Fund for the Doctoral Program of Higher Education (20090092120041).

## References

[1] K. Halbach, Nucl. Instrum. Meth. **169**, 1 (1980).
[2] Z. Q. Zhu, in Proc. Power Conversion Conf. Nagoya, Japan, K9 (2007).
[3] K. Atallah and D. Howe, IEEE Trans. Magn. **34**, 2060 (1998).
[4] T. Mizuno and H. Yamada, IEEE Trans. Magn. **28**, 3027 (1992).
[5] R. E. Clark, D. S. Smith, P. H. Mellor, and D. Howe, IEEE Trans. Magn. **31**, 3746 (1995).
[6] T. Mizuno and H. Yamada, EEE Trans. Magn. **28**, 3027 (1992).
[7] K. F. Rasmussen, H. D. John, T. J. E. Miller, M. I. McGilp, and O. Mircea, IEEE Trans. Magn. **36**, 1547 (2000).
[8] Z. Q. Zhu, Z. P. Xia, and D. Howe, IEEE Trans. Magn. **38**, 2997 (2002).
[9] N. Boules, IEEE Trans. Ind. Appl. **20**, 1267 (1984).
[10] N. Boules, IEEE Trans. Ind. Appl. **26**, 786 (1990).
[11] Z. Q. Zhu, D. Howe, E. Bolte, and B. Ackermann, IEEE Trans. Magn. **29**, 124 (1993).
[12] Z. Q. Zhu, David Howe, and C. C. Chan, IEEE Trans. Magn. **38**, 229 (2002).
[13] H. Wijono, H. Arof, and W. Ping, IET Electr. Power Appl. **4**, 629 (2010).
[14] D. L. Trumper, W. J. Kim, and M. E. Williams, IEEE Trans. Ind. Appl. **32**, 371 (1996).
[15] M. G. Lee, S. Q. Lee, and D. G. Gweon, Mechatronics **14**, 115 (2004).
[16] J. B. Wang and D. Howe, IEEE Trans. Magn. **41**, 2470 (2005).
[17] J. B. Wang, D. Howe, and G. W. Jewell, IEEE Trans. Magn. **39**, 3507 (2003).
[18] P. D. Pfister and Y. Perriard, IEEE Trans. Magn. **47**, 1739 (2011).
[19] X. H. Wang, Q. F. Li, and S. H. Wang, IEEE Trans. Magn. **18**, 424 (2003).
[20] R. P. Praveen, M. H. Ravichandran, V. T. S. Achari, V. P. J. Raj, G. Madhu, and G. R. Bindu, International Conference on Electrical Engineering/Electronics Computer Telecommunications and Information Technology (ECTI-CON), **19**, 254 (2010).
[21] A. B. Proca, A. Keyhani, A. El-Antably, W. Z. Lu, and M. Dai, IEEE Trans. Energy Conver. **18**, 386 (2003).
[22] Joon Hyuk Park, Jong Hyun Choi, Dong Ho Kim, and Yoon Su Baek, IEEE Trans. Magn. **40**, 3069 (2004).
[23] Seok-Myeong Jang, Min-Mo Koo, Yu-Seop Park, Jang-Young Choi, and Sung-Ho Lee, IEEE Trans. Magn. **47**, 3665 (2011).
[24] B. Ackermann and R. Sottek, Archiv fuer Elektrotechnik (Berlin) **78**, 117 (1992).
[25] Z. Q. Zhu and D. Howe, IEEE Trans. Magn. **29**, 143 (1993).
[26] D. C. Hanselman, New York: McGraw-Hill, Inc., 1994.